ELSEVIER

Inorganica Chimica Acta 339 (2002) 297–306

Inorganica Chimica Acta

www.elsevier.com/locate/ica

catena-[μ-Tris(1,2-bis(tetrazol-1-yl)ethane-N4,N4′)iron(II)] bis(tetrafluoroborate): synthesis, structure, spectroscopic and magnetic characterization of a chain-type coordination polymer spin-crossover compound

Johannes Schweifer [a], Peter Weinberger [a], Kurt Mereiter [b], Miro Boca [c], Christoph Reichl [d], Günter Wiesinger [d], Gerfried Hilscher [d], Petra J. van Koningsbruggen [e], Huub Kooijman [f], Matthias Grunert [a], Wolfgang Linert [a,*]

[a] *Institute for Applied Synthetic Chemistry, Vienna University of Technology, Getreidemarkt 9/163, A-1060 Vienna, Austria*
[b] *Institute for Chemical Technologies and Analytics, Vienna University of Technology, Getreidemarkt 9/164, A-1060 Vienna, Austria*
[c] *Institute for Inorganic Chemistry, Slovak Technical University, Radlinskeho 9, SK-81237 Bratislava, Slovakia*
[d] *Institute for Experimental Physics, Vienna University of Technology, Wiedner Hauptstraße 8-10/131, A-1040 Vienna, Austria*
[e] *Institute for Inorganic and Analytical Chemistry, Johannes-Gutenberg University, Staudingerweg 9, D-55099 Mainz, Germany*
[f] *Department of Crystal and Structural Chemistry, Bijvoet Center for Biomolecular Research, Utrecht University, Utrecht, Netherlands*

Received 12 November 2001; accepted 22 March 2002

Abstract

In analogy to a common synthesis of 1-substituted 5-H tetrazoles (Tetrahedron Lett. 36 (1995)1759; Beloruss. Gos. Univ., Minsk, USSR. Khim. Geterotsikl. Soedin. 11 (1985) 1521; Beloruss. Gos. Univ., Minsk, USSR. Khim. Geterotsikl. Soedin. 1 (1991) 66; BGU, Belarus. Vestsi Akad. Navuk Belarusi, Ser. Khim. Navuk 1 (1992) 73), the new bidentate ligand 1,2-bis(tetrazol-1-yl)ethane [endi] was synthesized and characterized by X-ray diffraction, NMR, IR and UV–Vis spectroscopy. By using iron(II) tetrafluoroborate hexahydrate the complexation with this ligand yields a 1-dimensional linear coordination polymer similar to the recently published chain compound (Inorg. Chem. 39 (2000) 1891) exhibiting a thermally induced spin-crossover phenomenon. Similar to the 1,2-bis(tetrazol-1-yl)propane-bridged compound, our 1,2-bis(tetrazol-1-yl)ethane-bridged compound shows a gradual spin transition, but the spin-crossover temperature $T_{1/2} \approx 140$ K is found to be 10 K above the other $T_{1/2}$. The $T_{1/2}$ was determined by temperature-dependent ^{57}Fe-Mössbauer, far FT-IR and UV–Vis spectroscopy as well as by temperature-dependent magnetic susceptibility measurements. Single crystals of the complex were grown in situ from a solution of the ligand and iron(II) tetrafluoroborate. The X-ray structure determinations of both the high spin as well as the low spin state of the compound revealed a solid state structure, which is comparable to that of *catena*-[Fe(1,2-bis(tetrazole-1-yl)propane)$_3$](ClO$_4$)$_2$ (Inorg. Chem. 39 (2000) 1891; 2nd TMR-TOSS Meeting, 4th Spin Crossover Family Meeting, Lufthansa Training Center, Seeheim/Germany, April 30–May 2, 1999). Both the 1,2-bis(tetrazol-1-yl)propane-bridged and our compound do not show a thermal hysteresis effect (J. Am. Chem. Soc. 115 (1993) 9810; Inorg. Chim. Acta 37 (1979) 169; Chem. Phys. Lett. 93 (1982) 567). The synthesis of the complex described in the experimental section yielded a fine powdered product being poorly soluble in most common solvents. The single crystal measurements were done with crystals obtained by various diffusion methods. Most of them yielded either thin needles or small hexagonal prism crystals depending on the specific conditions.

Keywords: Mössbauer; SQUID; X-ray diffraction; Far FT-IR; Spin transition; Iron(II) coordination polymer

1. Introduction

The first complexes of tetrazoles with iron(II) exhibiting spin crossover at temperatures below room temperature were synthesized by Franke et al. in 1982 [1]. In

Abbreviations: endi, 1,2-bis(tetrazol-1-yl)ethane.

* Corresponding author. Tel.: +43-1-58801 15350; fax: +43-1-58801 16299
E-mail address: wlinert@mail.zserv.tuwien.ac.at (W. Linert).

0020-1693/02/$ - see front matter © 2002 Elsevier Science B.V. All rights reserved.
PII: S0020-1693(02)00934-9

most of the cases, the spin transition between high and low spin can be observed optically by a change of color from white (or colorless) to an intensive violet–red [2]. Decurtins et al. [3] found the first LIESST effect with some of these compounds [4–6]. Simple 1-alkyl-substituted ligands can easily be obtained by the method of Satoh et al. [7] with yields of about 40–70%. Other methods [8–13] are found to be useful in special cases, if this simple preparation method fails. Monodentate ligands arrange themselves in an octahedral configuration around the iron center [14–16]. The coordinating atom of the tetrazole ring is generally the nitrogen atom at position 4. The donor number of tetrazole compounds was found to be quite low for compounds like (tetrazol-1-yl)propane and even lower for (tetrazol-1-yl)-2-halide–ethane. The stability of complexes is increased by the donor number and by an increasing number of coordination sites of the ligand, of course. Therefore, a possible step to obtain more stable spin crossover complexes is the synthesis of a chelating ligand consisting of two tetrazole rings bridged by alkyl chains of various chainlengths. In a first step we synthesized an ethylene-bridged compound. With this ligand we expected the formation of an octahedral complex with three bidentate ligands being attached to the iron center in a fashion that leads to a 3-dimensional network. The X-ray analysis revealed that obviously for sterical reasons 1,2-bis(tetrazol-1-yl)ethane [endi] acts as a bridging ligand between the iron(II) centers forming a 1-dimensional linear polymeric chain like the well known [Fe(4R-1,2,4-triazole)$_3$](anion)$_2$ systems [17–19].

2. Experimental

2.1. Reagents

Sodium azide 99% (Aldrich), triethyl orthoformate 99+% (ACROS), acetic acid 99.8% (Aldrich), 1,2-diaminoethan purum (LOBA Feinchemie), and iron-(II)tetrafluoroborate hexahydrate 97% (Aldrich) were used as supplied.

2.2. Synthesis of the ligand

The ligand 1,2-(tetrazol-1-yl)ethane [endi] was prepared similar to the method of Satoh et al. [7]. 1.8 g (30 mmol) of ethylenediamine, 11.8 g (80 mmol) of triethyl orthoformate and 5.2 g (80 mmol) of sodium azide were dissolved in 200 ml glacial acetic acid and stirred at 90 °C for 20 h. After cooling down to room temperature and keeping for 2 h the solvent was removed under reduced pressure. The crystalline product was then dissolved in 100 ml of water. Under vigorous stirring, a solution of 5N NaOH was added to increase the basicity of the solution to pH 9. After keeping for 5 h in the refrigerator at 5 °C, the crude product precipitates as colorless platelets, which are filtered off and washed with distilled water. The product is recrystallized from ethanol, washed and dried, yielding 53% of the theoretical amount. (*Anal.* Calc. for $C_4H_6N_8$: C, 28.92; H, 3.64; N, 67.44. Found: C, 29.08; H, 3.61; N, 66.57%), m.p. 132 °C.

NMR data: ^{1}H NMR (250.13 MHz, $CDCl_3$, δ (ppm)): 5.04 (s, 2H, –CH_2–CH_2–); 9.32 (s, 1H, 5H$_{tetrazole}$); ^{13}C NMR (62.86 MHz, $CDCl_3$, δ (ppm)): 46.6 (–CH$_2$–CH$_2$); 144.2 (5C$_{tetrazole}$).

Some characteristic absorptions in the mid-range FT-IR spectrum are the ν_{C-H} of the tetrazole carbon (3121 cm^{-1}) and the $\nu_{C=N}$ of the tetrazole ring (1811 cm^{-1}).

The far FT-IR spectrum of the ligand endi shows two characteristic vibrational modes due to vibrations involving all parts of the molecule at 387 and 367 cm^{-1}.

2.3. Synthesis of the complex [Fe(endi)$_3$](BF$_4$)$_2$

The complex (MW: 727.9) was synthesized in a dry nitrogen atmosphere. 0.997 g (6 mmol) of endi were dissolved in 30 ml of dry propylenecarbonate. 0.670 g (2 mmol) of iron(II) tetrafluoroborate hexahydrate were dissolved in 30 ml of absolute methanol. Both solutions were purged with dry nitrogen to remove the dissolved oxygen. Under stirring the solution of iron(II) tetrafluoroborate hexahydrate was slowly added to the solution of the ligand within 1 h. Subsequently, the mixture was heated to 45 °C and kept at this temperature for about 15 h. The amount of solvent is then decreased to approximately 30 ml under reduced pressure. The fine powdered colorless complex was filtered off and washed twice with cold ethanol and cold diethylether, and dried carefully in vacuo yielding 75% of the theoretical amount. The complex is poorly soluble in propylenecarbonate and pyridine. (*Anal.* Calc. for $C_{12}H_{18}B_2F_8FeN_{24}$: C, 19.80; H, 2.49; N, 46.18. Found: C, 20.59; H, 2.48; N, 44.66%.)

The *thermogravimetric analysis* confirms the absence of any solvent molecules in the compound (see Fig. 1).

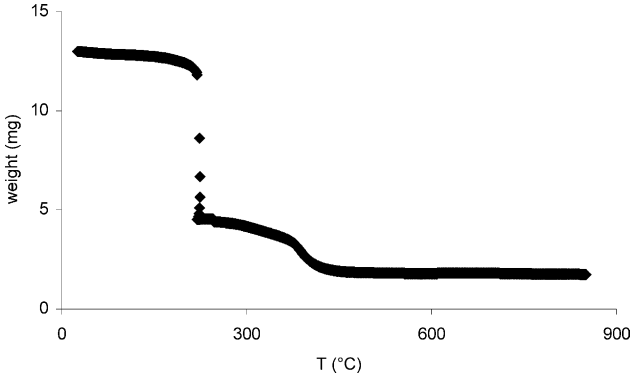

Fig. 1. Thermogravimetry of [Fe(endi)$_3$](BF$_4$)$_2$.

The loss of weight at a temperature of 100 °C is below 1% (i.e. below 7.3 g mol^{-1}). Furthermore, the good thermal stability of the complex is supported by the data showing that thermal degradation occurs slightly above 200 °C.

2.4. Preparation of single crystals of $[Fe(endi)_3](BF_4)_2$

For the X-ray analysis, several single crystals prepared by two methods have been used.

2.4.1. Method 1

The crystals were grown in situ by diffusion. 0.167 g (0.5 mmol) of iron(II) tetrafluoroborate hexahydrate were dissolved in 3 ml of absolute methanol and the resulting colorless solution was put in layer over a solution of 0.167 g (1 mmol) of endi in 6 ml of dry propylenecarbonate. To prevent the instant mixing of the two solutions the reaction was performed in a narrow reaction tube with a diameter less than 1.5 cm. After keeping the reaction tube in the dark for 30 days, the diffusion yielded very small needle-shaped crystals. The synthesis was performed with various molar ratios of iron(II)–tetrafluoroborate to endi like 1:2, 1:3, 2:3, 1:1 and 2:1, always yielding the same result.

2.4.2. Method 2

0.167 g (1 mmol) of endi and 0.167 g (0.5 mmol) of iron(II) tetrafluoroborate hexahydrate were separately dissolved in absolute methanol. Both solutions were filled together carefully in a reaction tube without stirring. For crystal growth the reaction tube was put into a sealed chamber containing absolute 2-propanol. The reaction tube was kept for 30 days in the dark yielding small prismatic hexagonal crystals.

2.5. Instrumentation

Elemental analyses were performed at the Institute for Inorganic Chemistry, Slovak Technical University, Bratislava (Slovakia). The characterization of the ligand was accomplished by NMR spectroscopy using a Bruker 250 FS FT NMR. Thermogravimetry was performed on a Shimadzu TGA-50 analyzer within the temperature range of 25–850 °C at a heating rate of 5 °C min^{-1}. Vibrational spectra were recorded on a Perkin–Elmer System 2000 far FT-IR and a Perkin–Elmer 16 PC mid-range FT-IR using a Graseby-Specac thermostatable sample holder with a Graseby-Specac automatic temperature controller within the temperature range of 100–298 K. UV–Vis spectra have been obtained on a World Precision Instruments S1000 fiber optic spectrometer with a diode array detector using the same thermostatable sample holder. All electronic spectra were automatically dark current-corrected. Single crystal X-ray diffraction data were measured with a Bruker SMART CCD diffractometer. In order to study also the low temperature behavior of the compound by X-ray diffraction, a Bruker Kryoflex nitrogen cooling device in conjunction with the SMART diffractometer was used to collect intensity data at 100, 150, and 200 K. For the determination of the magnetic susceptibility the powdered complex was pressed into pellets. Temperature-dependent magnetic susceptibility of the complex was measured with a superconduction interferometer device (SQUID) in external fields from 0.1 to 3 T. The ^{57}Fe-Mössbauer spectra were recorded between the temperature of liquid helium and room temperature using a conventional constant acceleration drive system. ^{57}Co in a Rh matrix with an activity of about 80 mCi was used as source. The data were analyzed using a least-squares fitting program and Lorentzian line shapes.

2.5.1. X-ray crystal structure determinations

The crystal structure of 1,2-bis(tetrazol-1-yl)ethane was determined at room temperature with a Bruker SMART diffractometer using standard procedures outlined in detail below. Important crystallographic data are given in Table 1.

For $[Fe(endi)_3](BF_4)_2$, a series of crystals was studied at room temperature with a Bruker SMART 3-circle diffractometer using a CCD area detector and graphite monochromatized Mo Kα radiation from a sealed X-ray tube. After omission of a limited number of very weak reflections, all these crystals consistently gave a primitive hexagonal unit cell with $a = 10.38$ Å and $c = 14.95$ Å at room temperature. However, they all showed significant streaks parallel to c^* of the reciprocal lattice for a part of the reflections with $l \neq 0$, whereas the reciprocal space near $hk0$ was free of streaks. This indicated the presence of some stacking disorder. In the lack of ordered crystals we decided to neglect these features and wished to derive an average structure model. For this purpose a colorless crystal ($0.09 \times 0.09 \times 0.35$ mm) terminated by smooth hexagonal prism

Table 1
Crystal and diffraction data for 1,2-bis(tetrazol-1-yl)ethane

Empirical formula	$C_4H_6N_8$
Formula weight	166.17
Crystal system	monoclinic
Space group	$P2_1/n$ (no. 14)
a (Å)	7.283(3)
b (Å)	5.450(2)
c (Å)	9.153(4)
β (°)	103.39(1)
V (Å^3)	353.4(2)
T (K)	296(2)
Z	2
μ(Mo Kα) (mm^{-1})	0.117
Reflections collected	2471
Independent reflections	997 ($R_{int} = 0.020$)
R_1 [$I > 2\sigma(I)$], wR_2, S	0.034 (811 refl.), 0.081, 0.92

faces and two uneven basal planes was used to record with the Bruker SMART diffractometer four frame sets (606 ω-scan frames with $\Delta\omega = 0.3°$ and $t = 43$ s per frame at $\varphi = 0$, 90, 180, and 270°, respectively) covering an entire sphere of the reciprocal space up to 0.71 $Å^{-1}$, i.e. $\theta_{max} = 30°$. These frame data were integrated by applying an optimized $2.7 \times 2.7 \times 0.7°$ integration window and continuously updated reflection profiles (program Bruker SAINT [20]). Absorption and related effects were corrected semi-empirically with program SADABS [20] assuming Laue symmetry 6/mmm (correction factors between 0.93 and 1.00). Data analysis with program XPREP [20] indicated centrosymmetry and gave $P\text{-}3c1$ as the most probable space group in which the structure was subsequently solved with direct methods. Other space groups were considered but were rejected for various reasons. After phase determination the Fourier synthesis showed an electron density distribution corresponding to a superposition of two mirror-related partial structures with common positions for Fe, B, and C2, whereas the tetrazole ring and the F atoms displayed approximately half-occupied split positions (see Fig. 4). In the subsequent least-squares refinement on F^2 with program SHELXL97 [21] this splitting was taken into account by introducing the following restraints: (i) The two tetrazole rings were forced to be flat and to have exactly the ring geometry as found in 1,2-bis(tetrazol-1-yl)ethane (Fig. 2), allowing only the ring positions and orientations to vary; (ii) the two crystallographically inequivalent Fe–N distances that previously gave values differing by 0.002 Å were restrained to refine to identical values; (iii) the $-CH_2-CH_2-$ groups linking pairs of tetrazole rings were set up to comply with both tetrazole ring orientations (unique carbon atom positions but CH_2 hydrogen atoms in two alternative orientations). Finally, an orientation disorder of the BF_4 tetrahedra with a single B and two sets of F atoms was taken into account without any geometric restraints. With this model, which included anisotropic temperature factors for all non-hydrogen atoms and isotropic ones for the hydrogen atoms (idealized positions according to the riding model), a chemically reasonable structure could be obtained and refined to satisfyingly low agreement indices given in Table 2. It should be noted that a refinement without restraints (i) and (ii) gave similar results with slightly better R-values but had the disadvantage that chemically equivalent bonds differed a little while being centered about their restrained counterparts. A model assuming twinning instead of split positions was also tested but did not show advantages from the chemical point of view. In order to also study the low temperature behavior of the compound by X-ray diffraction, a Bruker Kryoflex nitrogen cooling device in conjunction with the SMART diffractometer was used to collect intensity data at 100, 150, and 200 K in essentially the same fashion as described above, with the only exception that hemispheres instead of a complete sphere of the reciprocal space were harvested. The recorded diffraction images did not show any changes other than lattice contraction and reduced thermal displacements whereas the diffuse streaks remained unchanged. The restrained refinement model described above also proved to be useful for low temperature work and was retained after checking that a prefixed tetrazole ring geometry was justified by observing only negligible deviations when an unrestrained refinement model was used. Salient crystallographic data are compiled in Table 2.

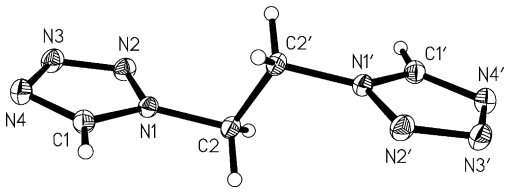

Fig. 2. Molecular structure of 1,2-bis(tetrazol-1-yl)ethane in the solid state (20% ellipsoids). Selected bond lengths and angles (Å, °): N1–C1 1.332(1), N1–N2 1.341(1), N1–C2 1.459(1), N2–N3 1.294(1), N3–N4 1.360(1), N4–C1 1.308(1), C2–C2′ 1.521(2), C1–N1–N2 108.4(1), C1–N1–C2 130.2(1), N2–N1–C2 121.4(1), N3–N2–N1 106.2(1), N2–N3–N4 110.8(1), C1–N4–N3 105.4(1), N4–C1–N1 109.2(1), N1–C2–C2′ 109.9(1).

3. Results and discussion

3.1. Crystal structures

3.1.1. 1,2-Bis(tetrazol-1-yl)ethane

The molecular structure of 1,2-bis(tetrazol-1-yl)ethane is shown in Fig. 2. The molecule is C_i symmetric with a *trans*-configuration of the two tetrazole rings relative to the ethylene bridge. Bond lengths and angles (Fig. 2) are in usual ranges. A packing diagram is shown in Fig. 3.

3.1.2. $[Fe(endi)_3](BF_4)_2$

The asymmetric unit of the structure is shown in Fig. 4. It consists of two sets of atoms that are related by pseudo-symmetry and distinguished by unprimed and primed atom names except for Fe and B which coincide for both sets. The refined site occupation factors for split positions were almost exactly 0.5, i.e. 0.498(3). For simplicity, the structure is first described in terms of the unprimed atoms while noting that the primed atoms practically define the mirror image of this structure. As shown in Fig. 5, the structure consists of iron atoms in octahedral coordination that alternate with three endi ligands to form cationic chains parallel to the crystallographic c-axis. The chains are in the ab plane arranged in a hexagonal close-packed fashion which leaves channel-like spaces in between occupied by the

Table 2
Crystal, diffraction, and geometric data for $[Fe(endi)_3](BF_4)_2$ at 296 to 100 K

T (K)	296(2)	200(1)	150(1)	100(1)
Diffraction data				
a (Å)	10.380(1)	10.293(1)	10.253(2)	10.178(2)
c (Å)	14.953(3)	14.921(3)	14.751(3)	14.586(4)
V (Å^3)	1395.3(3)	1368.9(3)	1342.9(5)	1308.6(4)
Color	colorless	colorless	red	red
D_{calc} (g cm^{-3})	1.733	1.766	1.800	1.848
Reflections collected	18421	13242	8392	7911
Independent reflections	1350	1306	1274	1262
R_{int}	0.031	0.033	0.048	0.039
Observed reflections [$I > 2\sigma(I)$]	1108	1050	987	1020
R_1, wR_2 [$I > 2\sigma(I)$]	0.048, 0.134	0.045, 0.111	0.049, 0.111	0.048, 0.109
R_1, wR_2	0.058, 0.143	0.057, 0.119	0.069, 0.123	0.061, 0.117
Selected geometric data (Å, °)				
Fe–Fe along c	7.477	7.461	7.376	7.293
Fe–N4 (6x)	2.182(1)	2.160(1)	2.095(2)	2.004(1)
N4–Fe–N4 (6x)	88.8(1)	89.0(1)	89.0(1)	89.3(1)
N4–Fe–N4 (6x)	91.2(1)	91.0(1)	91.0(1)	90.7(1)
N4–Fe–N4 (3x)	180.0	180.0	180.0	180.0
Fixed at all temperatures: C1–N1 1.332, N1–N2 1.341, N2–N3 1.294, N3–N4 1.360, N4–C1 1.308, N1–C2 1.459 Å				
C2–C2	1.452(4)	1.452(4)	1.450(5)	1.467(4)
B–F1	1.358(6)	1.352(4)	1.346(4)	1.343(4)
B–F3	1.356(6)	1.351(4)	1.344(4)	1.346(4)
B–F2	1.411(13)	1.445(9)	1.498(10)	1.507(8)
B–F4	1.419(13)	1.439(9)	1.498(9)	1.502(8)

Valid for all temperatures: Bruker SMART CCD diffractometer, chemical formula $C_{12}H_{18}B_2N_{24}F_8Fe$, $M_r = 727.9$, trigonal, space group $P\text{-}3c1$ (no. 165), $Z = 2$, $F(000) = 732$, λ(Mo Kα) = 0.71073 Å, μ(Mo Kα) $\approx$ 0.65 mm^{-1}, hexagonal prism 0.09 × 0.09 × 0.35 mm, data collection up to $\theta_{max} = 30°$, 131 parameters refined, 27 geometric restraints applied.

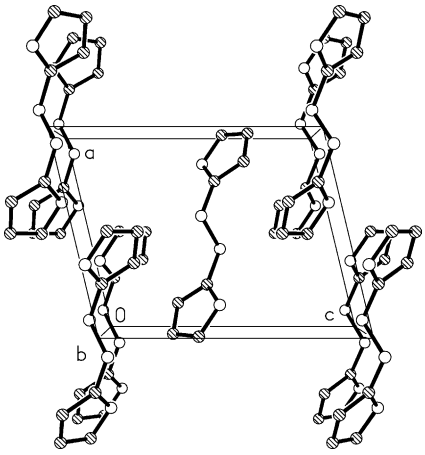

Fig. 3. Packing diagram of 1,2-bis(tetrazol-1-yl)ethane viewed along b.

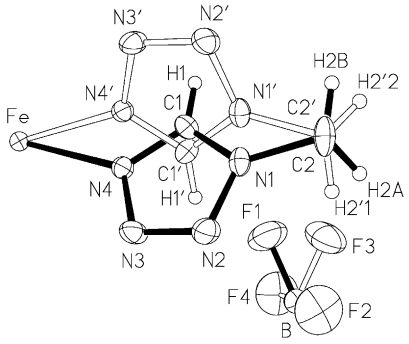

Fig. 4. Asymmetric unit of the structure of $[Fe(endi)_3](BF_4)_2$ ($T = 296$ K, 50% ellipsoids for non-hydrogen atoms) showing two alternatively occupied sets of atoms linked by full/open bonds, as used in the final structure refinement.

tetrahedral BF_4 anions (Fig. 6). Iron exhibits an almost undistorted octahedral coordination by six tetrazole nitrogen atoms. Whereas the N–Fe–N angles (about 89, 91 and by symmetry exactly 180°) vary little with temperature (Table 2), the Fe–N bond lengths are markedly temperature dependent: At room temperature the Fe–N bond length of 2.182(1) Å corresponds to a typical Fe^{2+} in high-spin state. After a small contraction to 2.160(1) Å at 200 K, there is a significant decrease to 2.095(2) Å at 150 K and to 2.004(1) Å at 100 K accompanied by a concomitant change from colorless (200 K) to red (150 and 100 K). The short Fe–N distance at 100 K is consistent with a largely complete transition into low-spin Fe^{2+}. This temperature dependence in Fe–N distances correlates well with the cell dimensions of which c, i.e. parallel to the cationic chains, is more sensitive than $a = b$. Thus, the intrachain Fe–Fe-distances are a good measure for the spin state. All other thermal changes in the structure remain small to insignificant, e.g. the C–C and the B–F bonds (verified also for C–N and N–N by test refinements

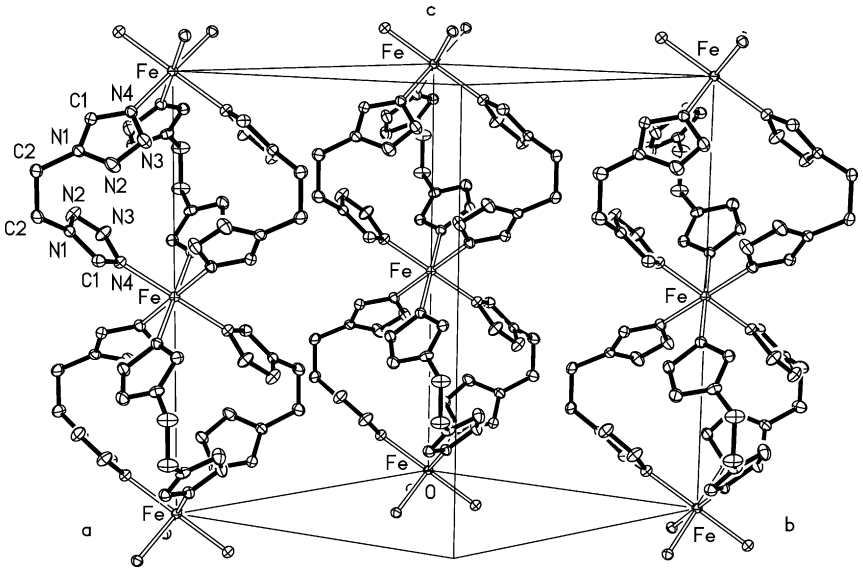

Fig. 5. Unit cell of $[Fe(endi)_3](BF_4)_2$ showing the chain-structure most clearly. Alternative orientation of the chains defined by primed atoms (Fig. 4) omitted for clarity.

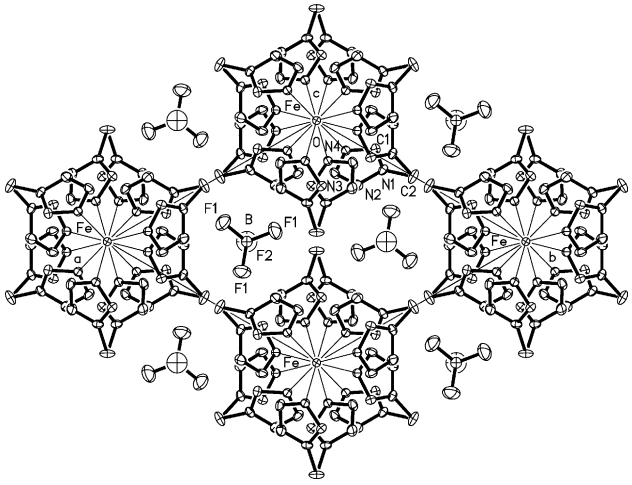

Fig. 6. Crystal structure of $[Fe(endi)_3](BF_4)_2$ in a projection down the *c*-axis.

without restraint (i), vide supra). The structure model presented here also permits a qualitative interpretation of the diffuse streaks in the diffraction pattern parallel to c^* of the reciprocal lattice. To this end we have to note that the primed atom positions shown in Fig. 4 practically coincide with the depicted unprimed atomic positions in the projection of Fig. 6. Thus, orientation mismatches of neighboring Fe–tetrazole chains will not produce diffuse streaks near *hk*0-reflections, exactly as observed, but will do so in three dimensions and off from *hk*0 reflections, as also observed.

The described structure of $[Fe(endi)_3](BF_4)_2$ corresponds essentially to that of $[Fe(btzp)_3](ClO_4)_2$ (btpz = 1,2-bis(tetrazol-1-yl)propane), which was reported to crystallize likewise in space group *P*-3*c*1 with cell dimensions of $a = 11.098(2)/11.030(2)$ Å and $c = 14.844(2)/14.546(2)$ Å at 200/100 K [22]. In comparison to $[Fe(endi)_3](BF_4)_2$, only one hydrogen atom per $-CH_2-CH_2-$ bridge has to be replaced by a methyl group and BF_4^- by ClO_4^-. For this compound, disorder of the terminal $-CH_3$ groups (alternatively attached to one of the two bridging carbon atoms) and of the ClO_4^- anion (two orientations similar to BF_4^- in $[Fe(endi)_3](BF_4)_2$) has been reported, whereas streaks indicating stacking faults were not specifically mentioned. It thus appears that the additional CH_3 groups in $[Fe(btzp)_3](ClO_4)_2$ prevent the Fe–tetrazole-chains from adopting two alternative and pseudo-symmetric orientations which for $[Fe(endi)_3](BF_4)_2$ have been addressed as the origin of visible diffuse features in the diffraction pattern. The Fe–N bond lengths in $[Fe(btzp)_3](ClO_4)_2$, 2.164(4) Å at 200 K, 2.038(4) at 100 K and the N–Fe–N bond angles (89, 91, and 180°) [22] compare well with corresponding values in $[Fe(endi)_3](BF_4)_2$ (Table 2).

3.2. Spectroscopic characterization

Mid-range FT-IR spectra of the ligand and the complex as KBr pellets have been recorded within the range of 4400–450 cm^{-1}. To accomplish a reasonable signal-to-noise ratio, 64 scans have been summed. The spectra are depicted in Fig. 7. The prominent absorption features in the mid-range IR of $[Fe(endi)_3](BF_4)_2$ are detected at 3155 cm^{-1} (stretching vibration ν_{C-H} at the tetrazole ring carbon), whereas the bands at 1507, 1454 and 1110 cm^{-1} are due to combinations of bond stretching vibrations typical for coordinated tetrazole rings. The bands at 1060 and 697 cm^{-1} are due to the asymmetric and the symmetric stretching vibration of the BF_4^- anion. The absorptions at 665 and 657 cm^{-1}

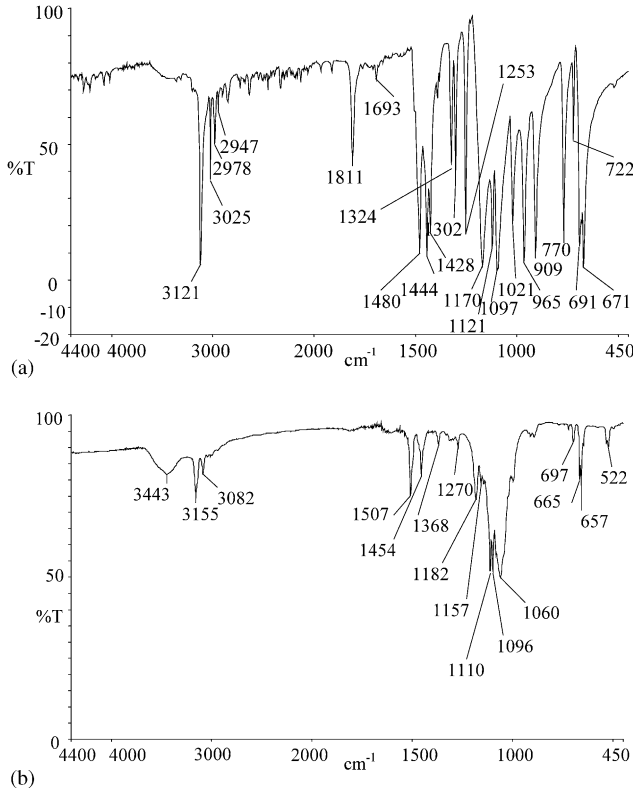

Fig. 7. Mid range FT-IR spectrum of the free ligand (a) and of $[Fe(endi)_3](BF_4)_2$ (b).

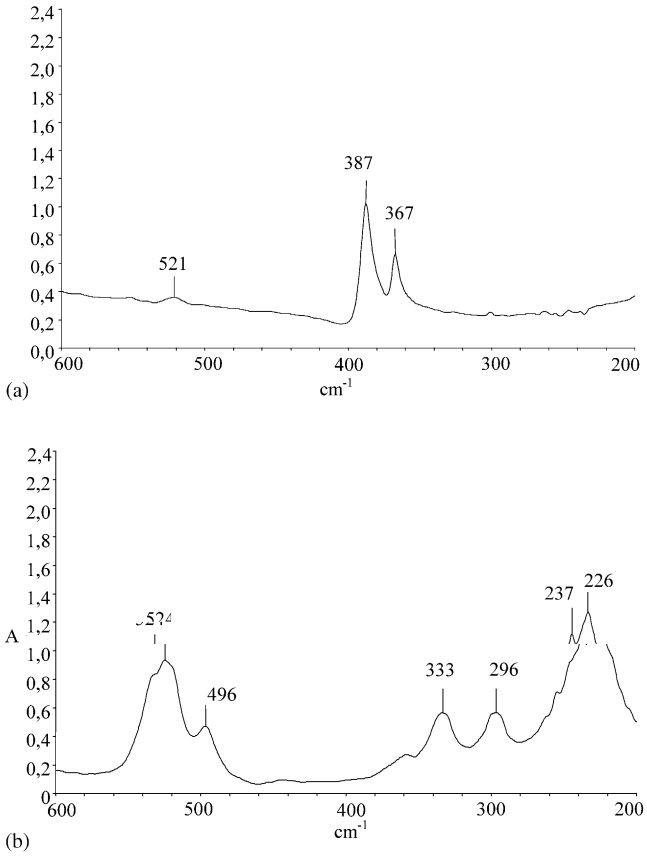

Fig. 8. Far FT-IR of the free ligand (a) and of $[Fe(endi)_3](BF_4)_2$ (b).

are typical for bond angle deformations of the coordinated tetrazole rings.

Far FT-IR spectra have been recorded as polyethylene pellets within the range of 600–200 cm^{-1}. To accomplish a reasonable signal-to-noise ratio, 1000 scans have been summed. The spectrum is depicted in Fig. 8.

The strong absorption at 524 cm^{-1} is due to an umbrella-like bond deformation of the BF_4^- counter anion, whereas the band at 333 cm^{-1} is assigned to a pairwise bending of BF_4^-. Due to the spin transition between a high and a low spin state of the iron(II), the ligand-to-metal bond is influenced regarding bond length and bond strength. This can be observed in the far IR region where the Fe–N stretching vibration is shifted dramatically from 296 cm^{-1} for the high spin complex towards 430 cm^{-1} for the low spin state. The temperature-dependent far FT-IR spectra are given in Fig. 9.

The change of the intensities of absorption (i.e. the peak area) at the frequencies of 300 and 430 cm^{-1} was evaluated and is plotted versus the temperature. These graphs in Fig. 10 show a higher spin transition temperature in comparison to the data derived by the measurements of the magnetic susceptibilities and Mössbauer spectra.

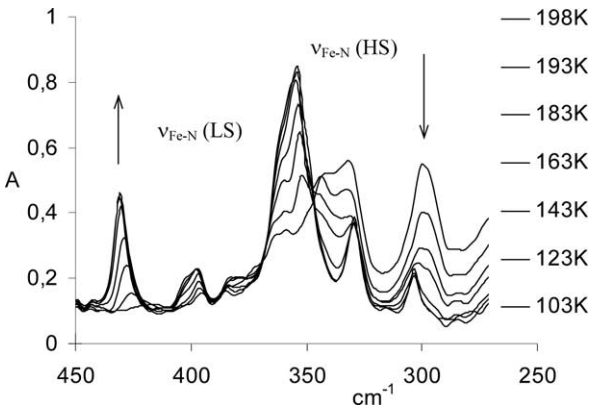

Fig. 9. Variable temperature far FT-IR spectra of $[Fe(endi)_3](BF_4)_2$.

The spin transition at the iron(II) coordination center changes the size of the energy gap between the d-orbitals thus altering the d-d transition energy. This change can be observed in temperature-dependent electronic spectra (see Fig. 11).

The variable temperature electronic spectra have been recorded in transmission mode using polyethylene pellets of $[Fe(endi)_3](BF_4)_2$ and a temperature range between 100 and 293 K in intervals of 10 K. To ensure reasonable thermostatization of the sample, the tem-

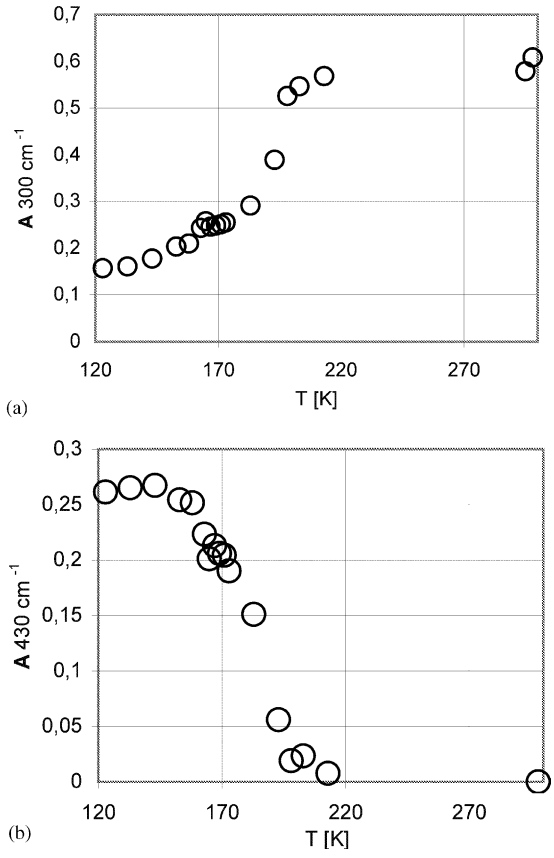

Fig. 10. Peak areas of the temperature-dependent far FT-IR spectra of $[Fe(endi)_3](BF_4)_2$ for ν_{Fe-N} (LS) (a), and for ν_{Fe-N} (HS) (b).

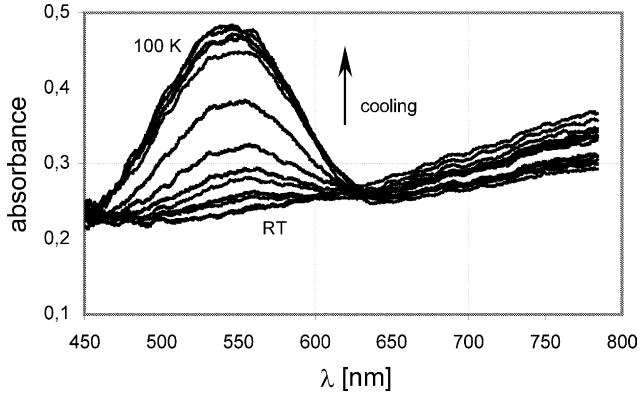

Fig. 11. Variable temperature electronic spectra of $[Fe(endi)_3](BF_4)_2$.

perature was kept constant for 10 min before the spectrum was recorded.

3.3. ^{57}Fe-Mössbauer studies

Finally, other independent evidence for the determination of the spin crossover temperature was obtained by temperature-dependent ^{57}Fe-Mössbauer spectroscopy confirming a $T_{1/2} \approx 140$ K, derived from the point of inflection of the relative subspectra intensity versus temperature curve. Mössbauer spectroscopy is a valuable tool for monitoring a spin transition. Since a spectrum reflects the splitting (shift) of the nuclear levels due to the quadrupole interaction (isomer shift), this particular technique can be used as a fingerprint method for identifying the different spin states (see Fig. 12.). In the spectrum displayed on top, representing the high spin phase, a small (7%) amount of an additional phase (iron(III)) is seen. Concerning the values for both isomer shift and quadrupole splitting, both patterns are typical for a ferrous high spin compound. On lowering the temperature at about 200 K, the first significant sign of a low spin component can be resolved from the background represented by a slightly broadened single line. Below that temperature both components are visible, the low spin pattern increasing on the expense of the high

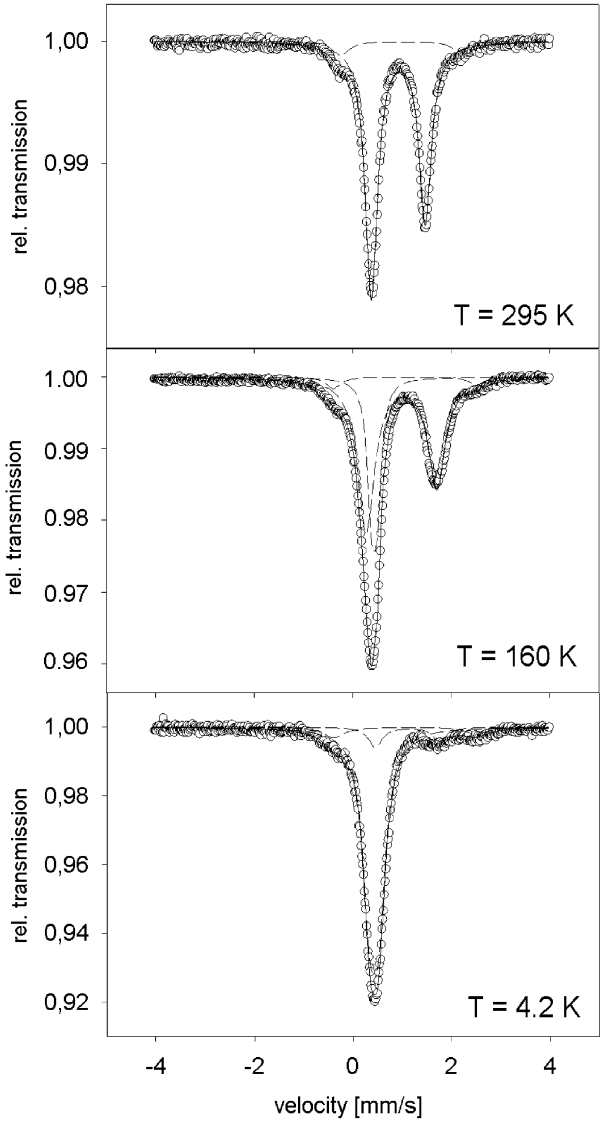

Fig. 12. ^{57}Fe-Mössbauer spectra of $[Fe(endi)_3](BF_4)_2$ for the high spin state (top), for an approximately equal amount of high spin and low spin complex (center), and for the low spin state (bottom).

spin pattern (see Fig. 12). Following the classification of Gütlich et al. [2], the present transition is a gradual one. Below 100 K the relative absorption area of the high spin compound drops below 10%, from whereon it essentially stays constant. From the spectrum recorded at 4.2 K (see Fig. 12, bottom) it is obvious that the low spin phase is dominant. The residual high spin fraction still present is indicative for the presence of defects and dislocations [2]. Both heating and cooling runs were performed, a significant hysteretic behavior, however, could not be detected which is in agreement with the results obtained from the other physical measurements. The temperature-dependent relative intensities for the high spin and the low spin state are given in Fig. 13. The intersection point of both curves in Fig. 13 confirms the $T_{1/2}$ of 140 K derived from magnetic data.

3.4. Magnetic characterization

Temperature-dependent magnetic susceptibility measurements have been performed in different fields (0.1, 1 and 3 T) which yield a good scaling of the susceptibility in this field range. The spin crossover temperature was found at about $T_{1/2} \approx 140$ K. The transition is rather gradual between $T = 100$ K and $T = 200$ K, and not complete as the low temperature value of χT per Fe(II) ion of 0.5 cm^3 K mol^{-1} shows (see Fig. 14). The analysis of the susceptibility in terms of a Curie Weiss law yields a reduction of the high temperature value to about 10–12% at low temperatures. According to Mössbauer spectroscopy, this is consistent with the remaining high spin fraction of about 9.3%. Under the assumption that the high spin–low spin ratio is independent of the sample preparation, the iron(III) content of this sample used for the susceptibility measurement is about 2%. Fig. 14b gives the corrected high spin to low spin ratio. The downturn at low temperatures can be attributed to the zero-field splitting of the residual Fe(II) high spin fraction.

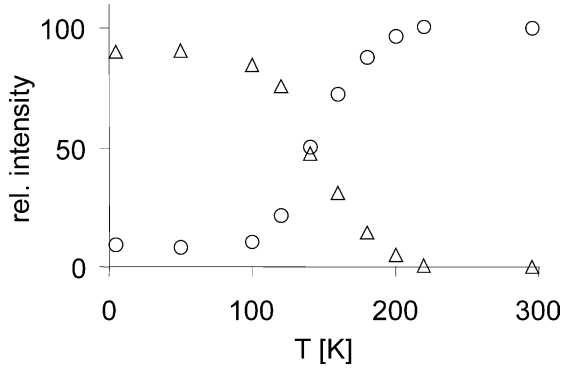

Fig. 13. Relative intensities of the ^{57}Fe-Mössbauer spectra of $[Fe(endi)_3](BF_4)_2$ for the high spin state (circles) and for the low spin state (triangle). The intersection point of both curves gives the $T_{1/2} \approx$

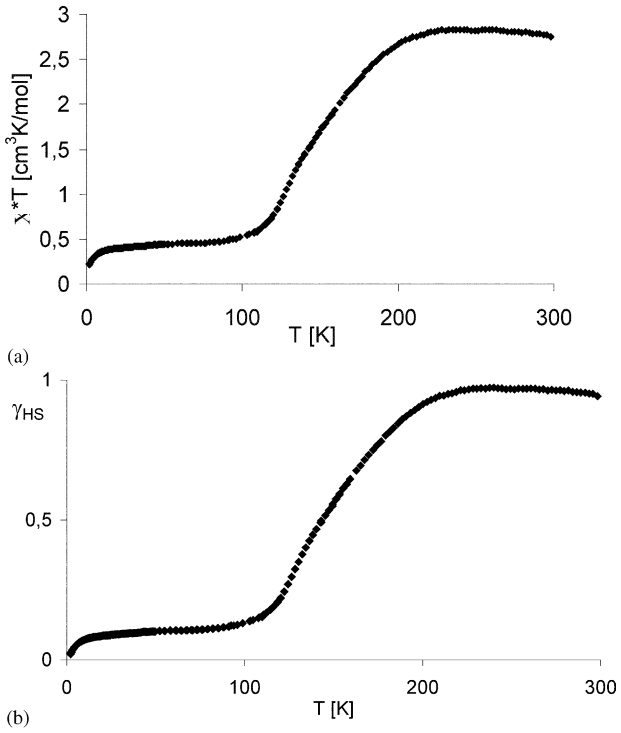

Fig. 14. Temperature-dependent magnetic susceptibility of the $[Fe(endi)_3](BF_4)_2$ complex (a) in an external field of 0.1 T; the corrected high spin–low spin ratio for iron(II) (b).

4. Conclusions

catena-[μ-Tris(1,2-bis(tetrazol-1-yl)ethane-N4,N4′) iron(II)] bis(tetrafluoroborate) is a structural analogue of the recently published *catena*-[μ-tris(1,2-bis(tetrazol-1-yl)propane-N4,N4′)iron(II)]bis(perchlorate) [22]. It exhibits a rather gradual spin transition which is not complete. The $T_{1/2}$ is about 140 K, which was verified by several independent methods. The Fe–Fe distance within the chain is approximately 7.5 Å. This is practically identical for both chain-type coordination polymers, $[Fe(endi)_3](BF_4)_2$ as well as $[Fe(btzp)_3](ClO_4)_2$. The slightly higher $T_{1/2}$ of our compound is attributable to the difference in the electron density distribution induced by the different alkyl bridges between the two tetrazole rings of the alkylditetrazoles. Introducing substituents decreasing the electron density at the ethylene bridge (e.g. halides) might shift the $T_{1/2}$ further towards room temperature. The gradual and incomplete spin transition occurs due to the fact that the chains are rather flexible, which leads on the one hand to disorder in the molecular structure and on the other hand to a kind of "shock absorber effect" thus lowering cooperative effects.

5. Supplementary material

Complete crystallographic data of all structures in this paper (excluding structure factors) have been deposited with the Cambridge Crystallographic Data Centre, CCDC Nos. 181857–181861. Copies of this information may be obtained free of charge from The Director, CCDC, 12 Union Road, Cambridge CB2 1EZ, UK (fax: +44-1223-336-033, email: deposit@ccdc.cam.ac.uk or www: http://www.ccdc.cam.ac.uk).

Acknowledgements

We thank Mr. J. Bauer for performing the thermogravimetric analysis. Thanks for financial support are due to the European Union for granting the TMR-project TOSS (Thermal and Optical Spin State Switching) under the contract ERB-FMRX-CT98-0199, to the European Science Foundation ESF for travel grants within the project "Molecular Magnets" as well as to the Austrian Science Foundation FWF ("Fonds zur Förderung der wissenschaftlichen Forschung in Österreich") for financial support within the project 11218-CHE and 13076-PHY. Thanks are also due to the "Hochschuljubiläumsfonds der Stadt Wien" for financial support within the project H-65/2000. M. Boca enjoyed financial support from the bilateral university partnership between the Vienna University of Technology and the Slovak Technical University.

References

[1] P.L. Franke, J.G. Haasnoot, A.P. Zuur, Inorg. Chim. Acta 59 (1982) 5.
[2] P. Gütlich, A. Hauser, H. Spiering, Angew. Chem. 106 (1994) 2109.
[3] S. Decurtins, P. Gütlich, C.P. Köhler, H. Spiering, A. Hauser, Chem. Phys. Lett. 105 (1984) 1.
[4] S. Decurtins, P. Gütlich, K. Hasselbach, H. Spiering, A. Hauser, Inorg. Chem. 24 (1985) 2174.
[5] S. Decurtins, P. Gütlich, C.P. Köhler, H. Spiering, J. Chem. Soc., Chem. Commun. (1985) 430.
[6] Th. Buchen, P. Gütlich, H.A. Goodwin, Inorg. Chem. 33 (1994) 573.
[7] Y. Satoh, Tetrahedron Lett. 36 (1995) 1759.
[8] E. Oliveri-Mandalá, B. Alagna, Ital. Gazz. Chem. 40II (1910) 441.
[9] P.A.S. Smith, N.W. Kalenda, J. Org. Chem. 23 (1958) 1599.
[10] G.A. Gareev, L.P. Kirillova, A.M. Belousov, N.S. Bukina, L.I. Vereshchagin, J. Org. Chem., USSR (1981) 1494.
[11] S.R. Buzilova, Y.V. Brekhov, A.V. Afonin, G.A. Gareev, L.I. Vereshchagin, J. Org. Chem., USSR 25 (1989) 1375.
[12] W.G. Finnegan, R.A. Henry, J. Org. Chem. 24 (1959) 1565.
[13] A.W. Addison, P.J. Burke, J. Heterocycl. Chem. (1981) 803.
[14] E.W. Mueller, J. Ensling, H. Spiering, P. Gütlich, Inorg. Chem. 22 (1983) 2074.
[15] R. Hinek, H. Spiering, D. Schollmeyer, P. Gütlich, A. Hauser, Chem. Eur. J. 2 (1996) 1427.
[16] L. Wiehl, Acta Crystallogr., B 49 (1993) 289.
[17] O. Kahn, C.J. Martinez, Science 279 (1988) 44.
[18] Y. Garcia, P.J. van Koningsbruggen, R. Lapouyade, L. Fournès, L. Rabardel, O. Kahn, V. Ksenofontov, S. Levchenko, P. Gütlich, Chem. Mater. 10 (1998) 2426.
[19] M. Verelst, L. Sommier, P. Lecante, A. Mosset, O. Kahn, Chem. Mater. 10 (1998) 980.
[20] Bruker, Programs SMART, version 5.054; SAINT, version 6.2.9; SADABS version 2.03; XPREP, version 5.1; SHELXTL, version 5.1. Bruker AXS Inc., Madison, WI, USA, 2001.
[21] G.M. Sheldrick, Programs SHELXS97 and SHELXL97, University of Göttingen, Göttingen, Germany, 1997.
[22] P.J. van Koningsbruggen, Y. Garcia, O. Kahn, L. Fournès, H. Kooijman, A.L. Spek, J.G. Haasnoot, J. Moscovici, K. Provost, A. Michalowicz, F. Renz, P. Gütlich, Inorg. Chem. 39 (2000) 1891.